Science
AAAS

Diisopropylammonium Bromide Is a High-Temperature Molecular Ferroelectric Crystal

Da-Wei Fu *et al.*

Science **339**, 425 (2013);
DOI: 10.1126/science.1229675

Science (print ISSN 0036-8075; online ISSN 1095-9203) is published weekly, except the last week in December, by the American Association for the Advancement of Science, 1200 New York Avenue NW, Washington, DC 20005.

SNAREs together, initiating trans-SNARE complex assembly in an NSF-SNAP–resistant manner; and (iv) the resulting Munc18-1–Munc13-SNARE assembly underlies the primed state that enables fast membrane fusion through the action of synaptotagmin-1 and Ca^{2+}.

The functional interplay between NSF-SNAPs and Munc18-1–Munc13 uncovered here suggests that in addition to their role in disassembling cis-SNARE complexes, NSF-SNAPs have an important function in guiding the system to the productive pathway by disassembling syntaxin-1–SNAP-25 heterodimers. This feature may arise because syntaxin-1–SNAP-25 heterodimers are heterogeneous and may constitute poor starting points for an exquisitely regulated process such as neurotransmitter release. In contrast, the syntaxin-1–Munc18-1 complex provides a well-defined starting point amenable to tight regulation by several factors, including Munc13 and other active zone proteins (*1*). This productive pathway may also be favored by specific interactions at active zones. Although some of these features are specific to synaptic vesicle fusion, multiple factors besides SNAREs are also required for physiological reconstitution of endosomal (*33*) and vacuolar (*34*) fusion. Moreover, the interplay between Munc18-1–Munc13 and NSF–α-SNAP is reminiscent of results obtained in reconstitutions of yeast vacuolar fusion, which showed that the homotypic fusion and vacuole protein sorting (HOPS) tethering complex orchestrates trans-SNARE complex assembly in an NSF-SNAP–resistant manner (*35*, *36*). It is remarkable that the same task can be performed by Munc18-1 and Munc13, even though HOPS includes an SM protein (Vps33p) and five large subunits without homology to Munc13. Thus, orchestration of SNARE complex assembly without interference from NSF-SNAPs may constitute a general function of SM proteins and associated factors. This notion does not preclude other functions proposed for SM proteins and their cofactors, including the possibility that they cooperate with the SNAREs in exerting force on the membranes to induce fusion (*10*, *37*).

References and Notes

1. J. Rizo, C. Rosenmund, *Nat. Struct. Mol. Biol.* **15**, 665 (2008).
2. T. C. Südhof, J. E. Rothman, *Science* **323**, 474 (2009).
3. T. Söllner, M. K. Bennett, S. W. Whiteheart, R. H. Scheller, J. E. Rothman, *Cell* **75**, 409 (1993).
4. P. I. Hanson, R. Roth, H. Morisaki, R. Jahn, J. E. Heuser, *Cell* **90**, 523 (1997).
5. R. B. Sutton, D. Fasshauer, R. Jahn, A. T. Brunger, *Nature* **395**, 347 (1998).
6. M. A. Poirier *et al.*, *Nat. Struct. Biol.* **5**, 765 (1998).
7. A. Mayer, W. Wickner, A. Haas, *Cell* **85**, 83 (1996).
8. I. Dulubova *et al.*, *EMBO J.* **18**, 4372 (1999).
9. K. M. Misura, R. H. Scheller, W. I. Weis, *Nature* **404**, 355 (2000).
10. I. Dulubova *et al.*, *Proc. Natl. Acad. Sci. U.S.A.* **104**, 2697 (2007).
11. J. Shen, D. C. Tareste, F. Paumet, J. E. Rothman, T. J. Melia, *Cell* **128**, 183 (2007).
12. J. Basu *et al.*, *Nat. Struct. Mol. Biol.* **12**, 1017 (2005).
13. C. Ma, W. Li, Y. Xu, J. Rizo, *Nat. Struct. Mol. Biol.* **18**, 542 (2011).
14. R. Fernández-Chacón *et al.*, *Nature* **410**, 41 (2001).
15. M. Verhage *et al.*, *Science* **287**, 864 (2000).
16. J. E. Richmond, W. S. Davis, E. M. Jorgensen, *Nat. Neurosci.* **2**, 959 (1999).
17. F. Varoqueaux *et al.*, *Proc. Natl. Acad. Sci. U.S.A.* **99**, 9037 (2002).
18. J. Pei, C. Ma, J. Rizo, N. V. Grishin, *J. Mol. Biol.* **391**, 509 (2009).
19. W. Li *et al.*, *Structure* **19**, 1443 (2011).
20. T. Weber *et al.*, *Cell* **92**, 759 (1998).
21. K. L. Boswell *et al.*, *J. Cell Biol.* **197**, 301 (2012).
22. M. C. Chicka, E. Hui, H. Liu, E. R. Chapman, *Nat. Struct. Mol. Biol.* **15**, 827 (2008).
23. A. Stein, A. Radhakrishnan, D. Riedel, D. Fasshauer, R. Jahn, *Nat. Struct. Mol. Biol.* **14**, 904 (2007).
24. M. Xue, C. Ma, T. K. Craig, C. Rosenmund, J. Rizo, *Nat. Struct. Mol. Biol.* **15**, 1160 (2008).
25. H. K. Lee *et al.*, *Science* **328**, 760 (2010).
26. Diao *et al.*, *eLife* **1**, e00109 (2012).
27. Materials and methods are available as supplementary materials on *Science* Online.
28. T. Weber *et al.*, *J. Cell Biol.* **149**, 1063 (2000).
29. R. Schneggenburger, E. Neher, *Curr. Opin. Neurobiol.* **15**, 266 (2005).
30. J. S. Rhee *et al.*, *Cell* **108**, 121 (2002).
31. O. H. Shin *et al.*, *Nat. Struct. Mol. Biol.* **17**, 280 (2010).
32. F. Deák *et al.*, *J. Cell Biol.* **184**, 751 (2009).
33. T. Ohya *et al.*, *Nature* **459**, 1091 (2009).
34. C. Stroupe, C. M. Hickey, J. Mima, A. S. Burfeind, W. Wickner, *Proc. Natl. Acad. Sci. U.S.A.* **106**, 17626 (2009).
35. J. Mima, C. M. Hickey, H. Xu, Y. Jun, W. Wickner, *EMBO J.* **27**, 2031 (2008).
36. H. Xu, Y. Jun, J. Thompson, J. Yates, W. Wickner, *EMBO J.* **29**, 1948 (2010).
37. J. Rizo, X. Chen, D. Araç, *Trends Cell Biol.* **16**, 339 (2006).

Acknowledgments: We thank Y. Sun for expert technical assistance; Y. Liu for initial efforts to reconstitute syntaxin-1–Munc18-1 complexes; and W. Li, W. Wickner, and M. Brown for fruitful discussions. This work was supported by grant I-1304 from the Welch Foundation (to J.R.), grant 31200618 from the National Science Foundation of China (to C.M.), and grants NS37200 and NS40944 from the NIH (to J.R.).

Supplementary Materials

www.sciencemag.org/cgi/content/full/science.1230473/DC1
Materials and Methods
Figs. S1 to S10
References (*38*–*57*)

19 September 2012; accepted 23 November 2012
Published online 20 December 2012;
10.1126/science.1230473

REPORTS

Diisopropylammonium Bromide Is a High-Temperature Molecular Ferroelectric Crystal

Da-Wei Fu,[1]* Hong-Ling Cai,[1]* Yuanming Liu,[2]* Qiong Ye,[1] Wen Zhang,[1] Yi Zhang,[1] Xue-Yuan Chen,[3] Gianluca Giovannetti,[4,5] Massimo Capone,[4] Jiangyu Li,[2]† Ren-Gen Xiong[1]†

Molecular ferroelectrics are highly desirable for their easy and environmentally friendly processing, light weight, and mechanical flexibility. We found that diisopropylammonium bromide (DIPAB), a molecular crystal processed from aqueous solution, is a ferroelectric with a spontaneous polarization of 23 microcoulombs per square centimeter [close to that of barium titanate (BTO)], high Curie temperature of 426 kelvin (above that of BTO), large dielectric constant, and low dielectric loss. DIPAB exhibits good piezoelectric response and well-defined ferroelectric domains. These attributes make it a molecular alternative to perovskite ferroelectrics and ferroelectric polymers in sensing, actuation, data storage, electro-optics, and molecular or flexible electronics.

Ferroelectrics are multifunctional electroactive materials with a range of applications. Their temperature-dependent spontaneous polarization can be switched by electric field or mechanical forces (*1*–*4*), making them attractive for temperature sensing, data storage, mechanical actuation, and energy harvesting (*5*). They often exhibit tunable dielectric responses and nonlinear electro-optic effects (*6*, *7*) and thus can also be used to manipulate electromagnetic waves (*1*). Ferroelectricity was originally discovered in Rochelle salt (*8*) in 1921 and later in a few other molecular systems (*9*), but the rapid development of ferroelectrics took place only after the discovery of ferroelectricity in perovskite barium titanate (BTO) (*10*) and lead zirconate titanate (PZT) (*11*). Relative to BTO and PZT, most

[1]Ordered Matter Science Research Centre, Southeast University, Nanjing 211189, China. [2]Department of Mechanical Engineering, University of Washington, Seattle, WA 98195, USA. [3]Fujian Institute of Research on the Structure of Matter, Chinese Academy of Sciences, Fuzhou 350002, China. [4]CNR-IOM-Democritos National Simulation Centre and International School for Advanced Studies (SISSA), Via Bonomea 265, I-34136 Trieste, Italy. [5]Institute for Theoretical Solid State Physics, IFW-Dresden, PF 270116, 01171 Dresden, Germany.

*These authors contributed equally to this work.
†To whom correspondence should be addressed. E-mail: xiongrg@seu.edu.cn (R.-G.X.); jjli@u.washington.edu (J.L.)

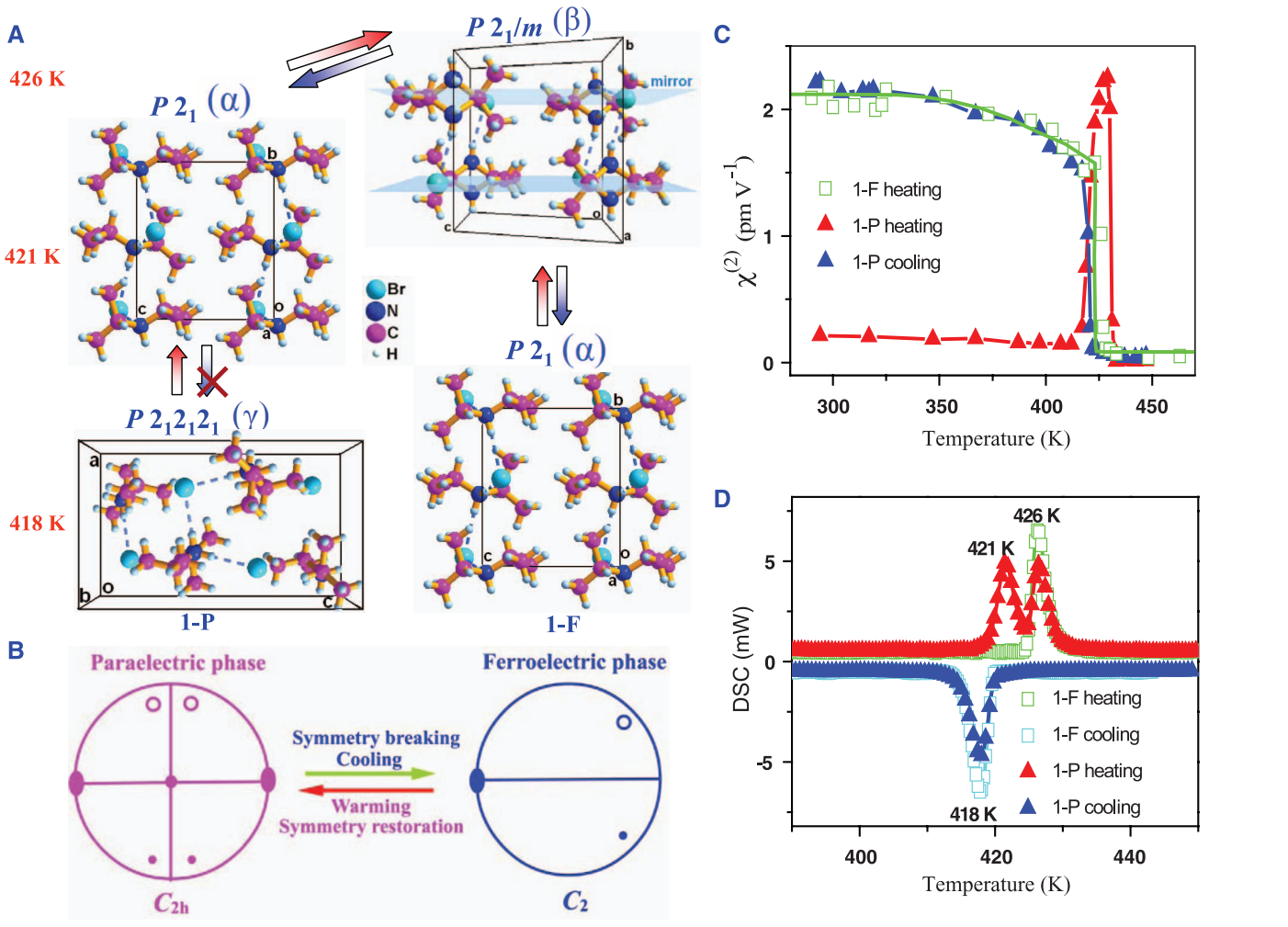

Fig. 1. Structural phase transition of DIPAB polymorphs. (**A**) The phase transition sequence: γ phase (1-P) to α phase at about 421 to 426 K (irreversible); α phase (1-F) to paraelectric β phase at 426 K (reversible). (**B**) Equatorial plane projection of point group of C_2 in the ferroelectric phase and C_{2h} in the paraelectric phase. (**C**) Second-order nonlinear optical coefficient versus temperature, confirming transition sequence seen in (A) and (B). (**D**) DSC data confirming transition sequence seen in (A) and (B).

Fig. 2. Dielectric properties of 1-F measured under different frequencies as a function of temperature. (**A**) Dielectric constant across the Curie point. (**B**) 1/ε′ follows the Curie-Weiss law. (**C**) Dielectric constant away from the Curie point. (**D**) The imaginary part of the dielectric constant.

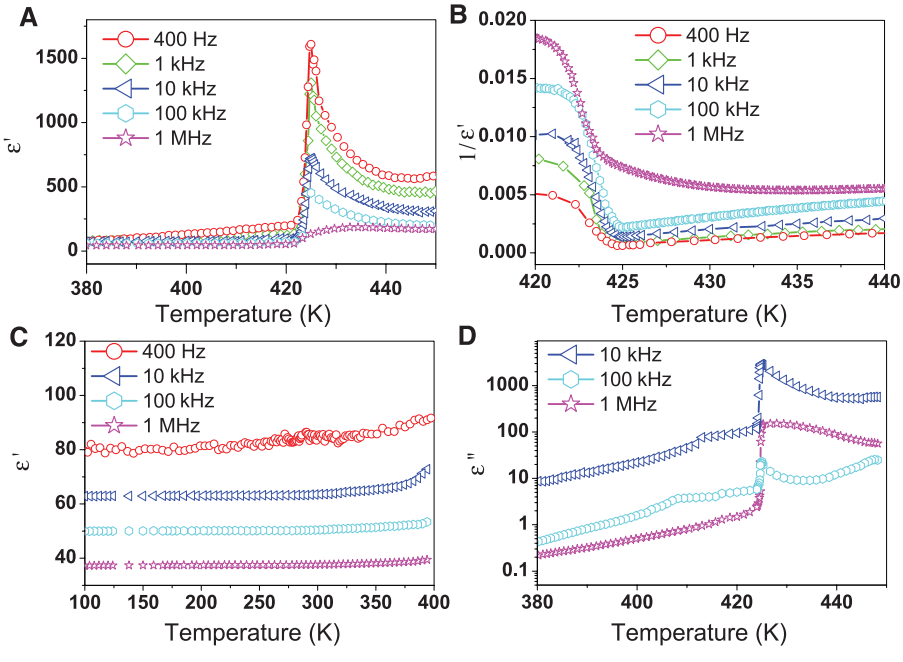

molecular ferroelectrics suffer from low spontaneous polarization (P_s), low melting temperature and phase transition temperature (Curie temperature, T_c), small dielectric constant, and weak piezoelectricity; their advantages include light weight, mechanical flexibility, and environmentally friendly processing as they are lead-free. Ferroelectric polymers such as poly(vinylidene fluoride) (PVDF) and its copolymers (*12*) share some of the drawbacks of molecular ferroelectrics, which limits their applications. The recently reported croconic acid (*6*) has a high spontaneous polarization of around 23 μC cm^{-2}; however, evidence for a ferroelectric phase transition, piezoelectric response, or ferroelectric domains has not been reported. By searching among organic compounds with a polar point group at room temperature and relatively high melting point, we found that diisopropylammonium chloride (DIPAC) is a ferroelectric with spontaneous polarization of 8.2 μC cm^{-2} (*13*). Here, we show that diisopropylammonium bromide (DIPAB), a molecular crystal processed from aqueous solution, possesses ferroelectric properties comparable to those of BTO.

A crystalline sample of DIPAB was grown by slow evaporation of the aqueous solution; the recrystallization of DIPAB yields two different polymorphs (*14*). One (1-F), obtained from methanol, is needle-shaped, whereas the other (1-P), obtained from water or a methanol-water solution, has a block shape (fig. S1). The 1-P form can be easily converted into 1-F by heating for 5 min at about 428 K, and large single crystals of 1-F suitable for dielectric hysteresis loop measurements can be obtained by controlling the cooling rate of the saturated methanol or aqueous solution of DIPAB.

Structure characterization by x-ray diffraction (XRD) (*14*) reveals that 1-F belongs to the monoclinic crystal system at room temperature, with a polar point group C_2 and chiral space group $P2_1$ (*15*) that we refer to as α phase (fig. S2 and table S1), which, in principle, is ferroelectrically active. In contrast, 1-P at room temperature belongs to the orthorhombic crystal system with a nonpolar point group D_2 and a chiral space group $P2_12_12_1$ (γ phase) (fig. S3 and table S2), which is ferroelectrically inactive. When the crystals were heated above 426 K (Fig. 1A), we observed that the nitrogen atoms of both polymorphs entered an apparently disordered state, resulting in a centrosymmetric structure with a nonpolar point group C_{2h} and space group $P2_1/m$ (β phase) (tables S1 and S2). When cooling down to room temperature, the space group of 1-F shifted back to $P2_1$, indicating a reversible phase transition. The space group of 1-P, on the other hand, became $P2_1$ instead of $P2_12_12_1$ upon cooling (Fig. 1A). Notably, a symmetric mirror plane disappeared below 426 K in α-DIPAB (Fig. 1B). Such broken symmetry has been verified by second harmonic generation (SHG) spectra, which are sensitive to the space inversion symmetry and thus are often used to detect ferroelectric transitions (*16*–*19*). The second-order nonlinear optical coefficient $\chi^{(2)}$ of 1-F (Fig. 1C) was close to zero above T_c and increased sharply below T_c, reaching a saturation value approximately twice that of KH_2PO_4 (KDP), a notable nonlinear optic crystal; this finding confirmed that the space inversion symmetry is broken at T_c. In the vicinity of T_c, $\chi^{(2)}$ showed a steplike jump indicating a first-order phase transition. The SHG effect of 1-P, on the other hand, was very weak at room temperature but increased sharply to an intensity very close to that of 1-F at 428 K; this is attributed to a transition from $P2_12_12_1$ to $P2_1$ upon heating. With further temperature increase, $\chi^{(2)}$ dropped rapidly to near zero, indicating transformation to centrosymmetric $P2_1/m$, and the subsequent cooling process revealed a variation of $\chi^{(2)}$ similar to that of 1-F. The SHG spectra thus are fully consistent with the phase transition sequence shown in Fig. 1A.

The phase transition sequences of 1-F and 1-P were further verified by differential scanning calorimetry (DSC) (Fig. 1D). Only one heat anomaly was observed for 1-F (at 418 to 426 K), suggesting a reversible phase transition. The sharp heat anomaly peak and a relatively large thermal hysteresis (8 K) are indicative of a first-order phase transition. This heat anomaly peak also can be observed in the differential thermal analysis (DTA) curve at about 423 K (fig. S4), showing that 1-F decomposes at about 520 K, far beyond T_c (*14*). For the 1-P crystal, there are two peaks, at 421 K and 426 K, in the heating process of the DSC measurement, and there is only one peak at 418 K in the cooling process. This is consistent with the crystal structure characterization and the SHG, and all the data combined suggest that in the heating process, the space group of 1-P is $P2_12_12_1$ below 421 K, possibly $P2_1$ between 421 K and 426 K, and $P2_1/m$ above 426 K, whereas in the cooling process it turns from $P2_1/m$ to $P2_1$ directly at 418 K. This type of polymorphism is rare in ferroelectric systems; consequently, in the temperature range between T_c and the liquid nitrogen boiling temperature, there is only one stable ferroelectric phase for DIPAB. In contrast, there are three ferroelectric phases for BTO in that temperature range. As such, DIPAB possesses one of the highest transition temperatures among molecular ferroelectrics at 426 K and

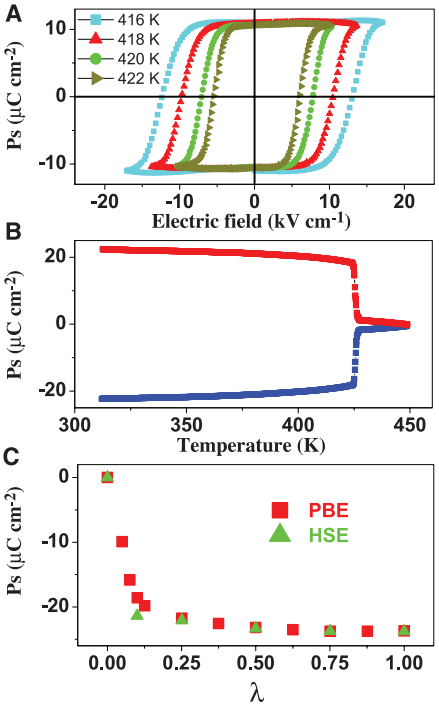

Fig. 3. Ferroelectric properties of 1-F. (**A**) Hysteresis loop measured at different temperatures. (**B**) Spontaneous polarization versus temperature. (**C**) Spontaneous polarization P_s along the path connecting the centrosymmetric $P2_1/m$ (λ = 0) to the experimental polar $P2_1$ structure (λ = 1), calculated from first principles using two different methods.

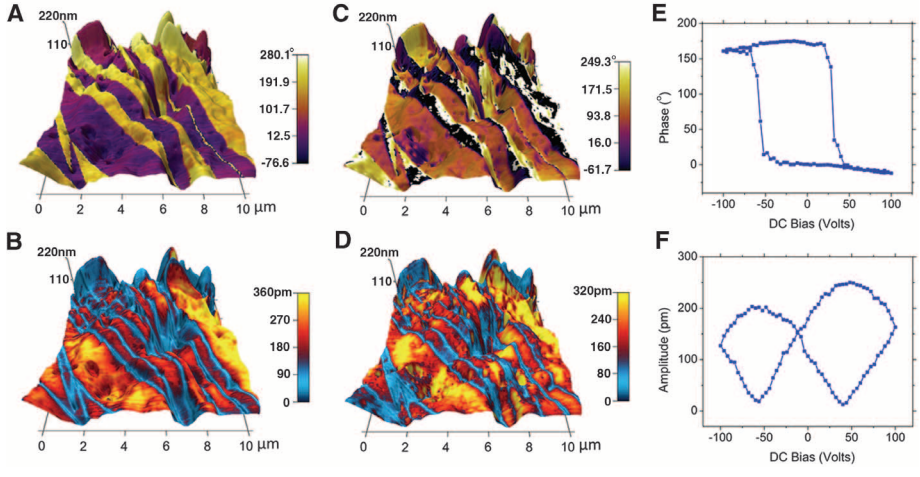

Fig. 4. Piezoresponse force microscopy of 1-F. (**A** and **B**) Phase mapping (A) and amplitude mapping (B) of vertical PFM overlaid on 3D topography. (**C** and **D**) Phase mapping (C) and amplitude mapping (D) of lateral PFM overlaid on 3D topography. (**E**) Phase-voltage hysteresis loop. (**F**) Amplitude-voltage butterfly loop.

has a stable structure in a broad temperature range below T_c, making it attractive for various applications.

A signature of the ferroelectric phase transition is a prominent dielectric anomaly. This is indeed observed at 426 K in the temperature dependence of the dielectric constant of 1-F (Fig. 2A), which shows a peak as high as 1608 at the lowest measured frequency. In the vicinity of T_c, the temperature-dependent permittivity along the polar axis follows the Curie-Weiss law of ferroelectric materials parameterized as $\varepsilon' = C/(T - T_0)$, as shown by the linear relationship between the reciprocal dielectric constant and the temperature in Fig. 2B. The Curie-Weiss constant C, a useful parameter for evaluating the value of P_s, is fitted to be 1.32×10^4 K, considerably higher than the values for ferroelectrics such as KDP (2.9×10^3 K) (*4*), triglycine sulfate (3.2×10^3 K) (*4*), $NaNO_2$ (4.7×10^3 K) (*4*), and DIPAC (8.4×10^3 K) (*13*), but smaller than that of inorganic compounds such as BTO (1.5×10^5 K) (*4*), $PbTiO_3$ (4.1×10^5 K) (*4*), and PZT (1.4×10^5 to 4.2×10^5 K) (*20*). The value of T_0 is estimated to be 416 K, smaller than T_c, indicating a first-order phase transition. In contrast, the temperature-dependent permittivity of 1-P shows an evident yet less prominent dielectric anomaly (fig. S5), which we were unable to fit to a Curie-Weiss form, reflecting its nonferroelectric nature (*14*). Far away from T_c, 1-F has a very large dielectric constant of up to 85 at room temperature measured under 400 Hz (Fig. 2C), an order of magnitude higher than that of polymer ferroelectrics such as PVDF. Even at a frequency of 1 MHz, the dielectric constant remains as high as 38, and its imaginary part ε'' is only 0.2 at 380 K (Fig. 2D), suggesting a small loss tangent of 0.44%. Such a high dielectric constant and low dielectric loss also make DIPAB attractive as a dielectric in capacitors for electric energy storage.

All the evidence points to a ferroelectric phase transition at 426 K in the 1-F polymorph, and indeed a ferroelectric hysteresis loop was recorded using a simple Sawyer-Tower circuit at 25 Hz. On cooling from 438 K, the 1-F loop looks like an open mouth–shaped ellipsoid (fig. S6), indicating paraelectric characteristics with leakage current (*14*). Just below T_c, a typical ferroelectric hysteresis loop emerges (Fig. 3A), confirming the ferroelectricity of α-DIPAB. The coercive field is estimated to be 5.0 kV cm^{-1}, smaller than those of PVDF (500 kV cm^{-1}) (*4*), BTO (10 kV cm^{-1}) (*4*), PZT (20 to 80 kV cm^{-1}) (*21*), and DIPAC (9 kV cm^{-1}) (*13*). The spontaneous polarization measured using a pyroelectric technique (Fig. 3B) reveals a very sharp transition from the paraelectric to the ferroelectric phase in an interval of about 3 K, indicating again a first-order phase transition. P_s is measured to be 23 μC cm^{-2}, compared to 8 μC cm^{-2} for PVDF (*4*), 26 μC cm^{-2} for BTO (*4*), 30 to 55 μC cm^{-2} for PZT (*21*), and 8 μC cm^{-2} for DIPAC (*13*). We also observed that the variation of P_s with respect to temperature is very similar to that of $\chi^{(2)}$, which can be explained from the relationship $\chi^{(2)} = 6\varepsilon_0\beta P_s$ deduced from Landau theory, where β is the high-order dielectric coefficient (*1*, *19*). To verify our measurement of spontaneous polarization, we performed first-principles density functional theory (*22*, *23*) calculations within the generalized gradient approximation to the exchange correlation potential according to the Perdew-Burke-Ernzerhof (PBE) method (*24*) and the Heyd-Scuseria-Ernzerhof hybrid (HSE) functional (*25*). The spontaneous polarization (Fig. 3C) is plotted as a function of the dimensionless variable λ (*14*), which parameterizes the continuous evolution from the centrosymmetric $P2_1/m$ structure (λ = 0), based on a supergroup analysis (*26*), to the experimental polar $P2_1$ structure (λ = 1); the agreement between these two approaches shows the stability and accuracy of the results. For the actual polar structure we obtain a finite polarization of ~23.9 μC cm^{-2}, in agreement with the experimental value. In addition, the abrupt variation of P_s as a function of λ also reflects the first-order phase transition observed in experiments. The calculations suggest that the emergence of the spontaneous polarization is driven by a cooperative atomic distortion at molecular sites that breaks the mirror symmetry plane of each single DIPAB molecule along the *b* axis of Fig. 1A, resulting in an asymmetric arrangement of the charges.

Finally, we used piezoresponse force microscopy (PFM) (*27*, *28*) to measure the local piezoelectric response and the ferroelectric domain structure at the nanoscale. Phase and amplitude mappings obtained with vertical PFM overlaid on three-dimensional (3D) topography (Fig. 4, A and B) correspond well to each other, revealing a ferroelectric domain pattern with alternating bands of upward and downward polarizations separated by domain walls; no crosstalk with topography is observed. The piezoresponse is measured to be as high as 360 pm under only 1 V ac, comparable with most other ferroelectrics, thus confirming its excellent piezoelectricity. Lateral PFM overlaid on 3D topography shows phase (Fig. 4C) and amplitude (Fig. 4D) mappings in good correspondence with the vertical mappings, despite the out-of-plane polarization direction of the sample. This can be understood from the piezoelectric tensor **d** of a C_2 point group, with nonzero d_{22} and d_{25} and spontaneous polarization P_2 (*29*), which induces normal and shear piezoelectric strains simultaneously under an electric field applied along the polar axis, whereas for BTO and PZT with out-of-plane polarization, only normal response is expected from symmetry. In this sense, the terms vertical and lateral PFM are somewhat misleading, and it is more appropriate to describe the data in terms of normal and shear PFM. Switching PFM was also carried out, with dc voltage applied on top of the ac voltage to switch the polarization, resulting in characteristic hysteresis and butterfly loops (Fig. 4, E and F). These findings further confirm the ferroelectricity of the molecular crystal.

References and Notes

1. M. E. Lines, A. M. Glass, *Principles and Applications of Ferroelectrics and Related Materials* (Oxford Univ. Press, New York, 2001).
2. W. Zhang, R. G. Xiong, *Chem. Rev.* **112**, 1163 (2012).
3. W. Eerenstein, N. D. Mathur, J. F. Scott, *Nature* **442**, 759 (2006).
4. S. Horiuchi, Y. Tokura, *Nat. Mater.* **7**, 357 (2008).
5. J. F. Scott, *Science* **315**, 954 (2007).
6. S. Horiuchi *et al.*, *Nature* **463**, 789 (2010).
7. M. Veithen, X. Gonze, P. Ghosez, *Phys. Rev. Lett.* **93**, 187401 (2004).
8. J. Valasek, *Phys. Rev.* **17**, 475 (1921).
9. A. Lurio, E. Stern, *J. Appl. Phys.* **31**, 1125 (1960).
10. H. D. Megaw, *Nature* **155**, 484 (1945).
11. B. Jaffe, R. S. Roth, S. Marzullo, *J. Appl. Phys.* **25**, 809 (1954).
12. A. J. Lovinger, *Science* **220**, 1115 (1983).
13. D.-W. Fu *et al.*, *Adv. Mater.* **23**, 5658 (2011).
14. See supplementary materials on *Science* Online.
15. G. Kociok-Köhn, B. Lungwitz, A. C. Filippou, *Acta Crystallogr. C* **52**, 2309 (1996).
16. J. H. Lee *et al.*, *Nature* **466**, 954 (2010).
17. M. Fiebig, Th. Lottermoser, D. Fröhlich, A. V. Goltsev, R. V. Pisarev, *Nature* **419**, 818 (2002).
18. C. C. Neacsu, B. B. van Aken, M. Fiebig, M. B. Raschke, *Phys. Rev. B* **79**, 100107 (2009).
19. H.-L. Cai *et al.*, *Phys. Rev. Lett.* **107**, 147601 (2011).
20. I. Kanno, Y. Yokoyama, H. Kotera, K. Wasa, *Phys. Rev. B* **69**, 064103 (2004).
21. C. M. Foster *et al.*, *J. Appl. Phys.* **81**, 2349 (1997).
22. G. Giovannetti *et al.*, *Nat. Commun.* **2**, 398 (2011).
23. P. Hohenberg, W. Kohn, *Phys. Rev.* **136** (3B), B864 (1964).
24. J. P. Perdew, K. Burke, M. Ernzerhof, *Phys. Rev. Lett.* **77**, 3865 (1996).
25. J. Heyd, G. E. Scuseria, M. Ernzerhof, *J. Chem. Phys.* **118**, 8207 (2003).
26. E. Kroumova *et al.*, *J. Appl. Cryst.* **34**, 783 (2001).
27. S. V. Kalinin *et al.*, *Annu. Rev. Mater. Res.* **37**, 189 (2007).
28. D. A. Bonnell, S. V. Kalinin, A. L. Kholkin, A. Gruverman, *MRS Bull.* **34**, 648 (2009).
29. J. F. Nye, *Physical Properties of Crystals: Their Representation by Tensors and Matrices* (Oxford Univ. Press, New York, 1985).

Acknowledgments: Supported by NSFC key fund grants 20931002 and 90922005 (R.-G.X.), NSF grant CMMI 1100339 (J.L.), and the European Research Council under starting independent research grant 240524 "SUPERBAD" (M.C. and G.G.). Numerical calculations were performed at CINECA. J.L. and R.-G.X. contributed to the design of the study, analysis of the data, and writing of the paper. D.-W.F. did the sample preparation. H.-L.C. made the dielectric constant and ferroelectric hysteresis loop measurements. Y.L. did the PFM studies. W.Z. wrote parts of the paper. Q.Y. contributed ideas and wrote some key parts of the paper. Y.Z. carried out the powder diffraction studies. X.-Y.C. carried out SHG measurements. G.G. and M.C. made ab initio calculations and wrote part of the manuscript.

Supplementary Materials

www.sciencemag.org/cgi/content/full/339/6118/425/DC1
Materials and Methods
Figs. S1 to S6
Tables S1 and S2
References (*30*–*33*)

4 September 2012; accepted 14 November 2012
10.1126/science.1229675